Front. Phys., 2012, 7(2): 160–164
DOI 10.1007/s11467-011-0196-x

RESEARCH ARTICLE

Tuning the Fermi level in Bi_2Se_3 bulk materials and transport devices

Zhi-yong Wang, Peng Wei, Jing Shi†

Department of Physics & Astronomy, University of California, Riverside, CA 92521, USA

E-mail: †jsjshi@gmail.com

Received May 17, 2011; accepted June 30, 2011

Bi_2Se_3 has been predicted to be a three-dimensional (3D) topological insulator (TI) with Dirac fermions residing on the two-dimensional (2D) surface. Unique transport properties such as high carrier mobility due to the suppressed backscattering are expected for the Dirac fermions. In order to eliminate the contribution of the bulk carriers, therefore, to place the Fermi level in the band gap of Bi_2Se_3, we first introduce various amounts of Ca dopants into the crystal to realize the bulk insulating state. Then by avoiding uncontrolled heating and electron beam irradiation in the nanofabrication process, we maintain the insulating state in thin devices. By sweeping the gate voltage, we have observed a conductivity minimum that is expected for the Dirac fermions in the band gap of 3D TIs.

Keywords topological insulators, Bi_2Se_3, transport properties, nano-devices

PACS numbers 73.63.-b, 72.20.-i

Bi_2Se_3, among other materials, has been predicted to be a 3D topological insulator candidate [1]. Its large band gap (∼0.3 eV at zero temperature) and the relatively simple band structure, i.e. having a single Dirac cone, make it a very attractive material for both fundamental physics studies and potential technological applications. The predicted characteristic Dirac spectrum and the chiral spin states have been confirmed by photoemission experiments [2, 3]. In addition, the forbidden backscattering of the surface Dirac fermion states has also been confirmed by scanning tunneling microscopy [4]. These spectroscopic techniques probe the surface states that even coexist with an overwhelmingly large density of the bulk states, and therefore insulator samples are not strictly required. Dirac fermions residing on the topological insulator (TI) surface are expected to have unique transport consequences such as high carrier mobility due to the suppressed backscattering. In order to study the transport properties of TI, however, the bulk contribution to the electrical conductivity needs to be minimized or eliminated because both channels conduct in parallel. If the Fermi level lies in the bulk band, either the conduction or valence band, the conductivity is predominantly metallic due to the large density of the bulk carriers.

It is generally believed that Se vacancies in Bi_2Se_3 introduce a large density of electrons even in the nominally stoichoimetric material [5], which places the Fermi level in the conduction band and leads to the co-existence of the surface and bulk carriers in the same materials [6, 7]. In bulk samples, the total number of 3D carriers is much greater than that of the 2D surface carriers. This has been a major hurdle in studying transport properties of the surface states of TIs. In this paper, we describe a pathway to prepare insulating devices for electrical transport studies. First we control the carrier type and carrier density in high-quality bulk Bi_2Se_3 crystals by introducing p-type dopants, i.e., Ca. Then we repeatedly cleave the optimally doped crystals to exfoliate thin flakes, which reduces the bulk/surface carrier ratio. We use a nanofabrication-free method to minimize the effects of nanofabrication processes such as baking and electron beam irradiation. Finally, we fine tune the remaining carrier density in the insulating devices by electrostatic gating, which controls the Fermi level position inside the band gap. The observed conductivity minimum is attributed to the Dirac point of a surface layer in the bulk bandgap of Bi_2Se_3.

We adopt a multi-step heating method to grow Ca-doped Bi_2Se_3 single crystals [5, 8]. The Ca atoms are expected to replace the Bi atoms and supply holes to the host. High purity (99.999%, from Alfa Aesar) stoichoimetric Bi_2Se_3 compound and a certain amount of

©Higher Education Press and Springer-Verlag Berlin Heidelberg 2012

Ca (99.98%, from Alfa Aesar) are put into a quartz tube that is sealed in vacuum. Then the quartz tube is put into a programmable furnace which is heated to 800℃ and kept at this temperature for 24 hours. Afterwards, it is cooled to and kept at 500℃ for 72 hours before it is cooled down to room temperature naturally. All crystals grown this way can be easily cleaved, indicating good quality of the materials (Fig. 1).

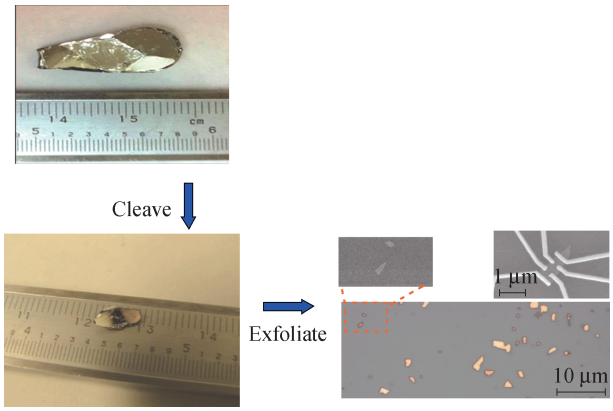

Fig. 1 A single crystal grown by the multiple-step heating method described in the text. The crystal can be easily cleaved into pieces with flat and shining surfaces. For this work, thin flakes are formed by exfoliation as indicated by optical microscope and scanning electron microscope images. Thin and small flakes are chosen for nanofabrication of devices.

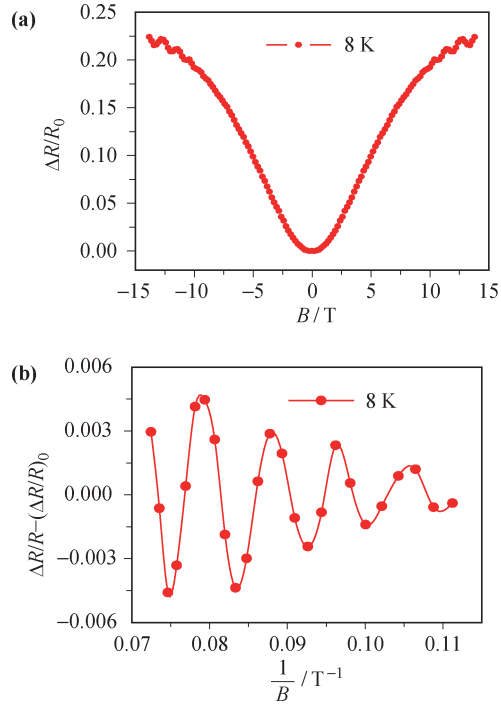

Fig. 2 **(a)** Magnetoresistance, or $MR = [R(B) - R(0)]/R(0)$, of an undoped Bi_2Se_3 crystal measured at 8 K. The Shubnikov–de Haas (SdH) oscillations of the resistance are clearly seen at high fields. **(b)** The same SdH data (a smooth background is removed) are plotted as a function of $1/B$.

All undoped crystals are n-type, with typical electron concentration about 5×10^{18} cm^{-3}. The room temperature resistivity is ~ 1 mΩ·cm, with strong metallic temperature dependence, i.e., the resistivity decreases as the temperature is lowered. The magnetoresistance of an undoped sample is shown in Fig. 2(a). Clear Shubnikov—de Haas (SdH) oscillations can be identified at $T = 8$ K for magnetic fields above 10 T. Figure 2(b) shows the data after the background is removed. The carrier density calculated from the SdH oscillations agrees well with the Hall effect data. As Ca-dopants are introduced, the net carrier density decreases systematically, indicating that more Ca atoms have replaced Bi atoms and created holes. At $x = 1.2\%$ ($Bi_{2-x}Ca_xSe_3$), the carrier density reaches its minimum, accompanied by a maximum in resistivity. With higher Ca-doping levels, the carrier type changes from n- to p-type, as confirmed by the Hall effect data. These facts clearly indicate that a fraction of Ca atoms originally put in the crystal have substituted Bi atoms in the host, which causes carrier compensation at $x = 1.2\%$.

Clearly, the Ca-doping results in a Fermi level downshift in the conduction band first and then a crossover to the valence band. To characterize the Fermi level position, we have carried out systematic infrared measurements to determine the absorption energy due to the electron inter-band transition. Both the transmittance and reflectance data are simultaneously recorded and the transmittance spectra are shown in Fig. 3(c). For the transmission geometry, the thickness ranges from 10 to 100 μm so that sufficient light can pass through the sample in the band gap. From the transmittance data, it is relatively straightforward to identify the absorption edge due to the inter-band transition. This energy has a minimum at $x = 1.2\%$, confirming that $x = 1.2\%$ is the compensation point where the crossover in the carrier type occurs [Fig. 3(b)]. In both transmittance and reflectance spectra, the periodic oscillations are caused by the Fabry–Perot interference between two flat cleaved surfaces. From the carrier density dependence of the inter-band transition energy that is a function of the Fermi energy and the effective mass of electrons and holes, we can determine the band gap at room temperature and the reduced effective mass [8]. Both are in reasonable agreement with the reported data in literature [10, 11]. Listed in Table 1 are the carrier density, room temperature electrical resistivity, and the energy of the onset of inter-band transition measured from the infrared transmittance spectra for four representative samples.

At x=1.2%, the resistivity of the samples is apparently insulating like, i.e., the resistivity decreases as the temperature is raised [Fig. 3(a)]. The room temperature resistivity value is nearly two orders of magnitude larger than that of the metallic samples with higher or lower Ca-doping. Hence, by controlling Ca-doping, we can tune the position of the Fermi level in bulk crystals from the conduction band, through the band gap, to the

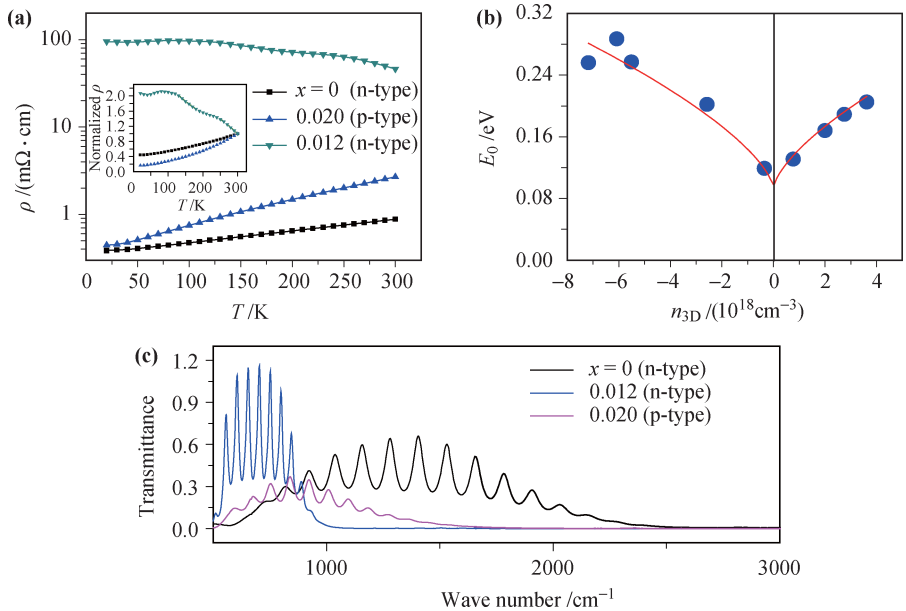

Fig. 3 **(a)** Electrical resistivity of three representative samples: undoped, x=0.012 and x=0.020. The inset shows the same data scaled by the resistivity at 300 K. **(b)** Absorption energy at the onset of the inter-band transition (determined from the spectra below) vs. carrier density for both n- and p-type crystals. The minimum energy corresponds to x=0.012, the optimal doping. **(c)** Representative transmittance spectra from the same three samples whose resistivity data are shown in (a).

Table 1 Room temperature carrier density (measured by the van der Pauw method), room temperature resistivity, and onset of inter-band transition energy for four representative Ca doping levels.

x in $Ca_xBi_{2-x}Se_3$	Room temperature carrier density /cm^{-3}	Room temperature resistivity /(mΩ·cm)	Onset of inter-band transition energy /eV
0	-5.13×10^{18}	0.88	0.286
0.005	-5.60×10^{18}	0.94	0.246
0.012	-3.52×10^{17}	46	0.119
0.020	$+3.62\times10^{18}$	2.69	0.205

valence band. Our measurements confirm that the bulk insulating state can be achieved with the optimal doping at $x \sim 1.2\%$.

The detailed temperature dependence of the resistivity of optimally doped samples is quite complex. The insulating-like resistivity generally shows two kinks and saturates at low temperatures. In some samples, the activated behavior across two distinct energy gaps can be fitted to the double-kink feature. Although not every temperature-dependent resistivity curve can be quantitatively analyzed well with this picture, at the optimal doping, the insulating-like resistivity suggests that the Fermi level lies in the band gap.

In the optimally Ca-doped Bi_2Se_3 crystals, further tuning of the Fermi level position in the band gap is expected by electrostatic gating. We adopt similar procedures used for preparing gate tunable graphene devices. We first obtain Bi_2Se_3 thin flakes by repeated cleaving or exfoliation. We place the flakes on a SiO_2(300 nm)/Si wafer in which the degenerately doped Si substrate serves as the back gate. In general, the thinner the flakes are, the smaller the size of the flakes is. The thickness of the flakes is determined by atomic force microscopy. Usually the thinner flakes (from 10 to 50 nm) can be easily distinguished from thicker ones by the contrast in optical microscopy images (Fig. 1). The typical lateral size of the relatively thin flakes is $\sim$ 10 μm or less. Having identified desired flakes, we use electron beam lithography (EBL) to fabricate transport devices. A typical EBL device is shown in Fig. 4(a). In almost all devices we have prepared with EBL, however, we find that the resistivity vs. temperature curve shows a metallic behavior [Fig. 5(a)]. As the gate voltage is swept from negative to positive, the resistance monotonically decreases [Fig. 5(b)], indicating an n-type behavior. Furthermore, the relative resistance change is very small (less than 20%). These facts suggest that the excess electrons are introduced in the nanofabrication process. The electron density increase was reported previously [9] due to the exposure of Bi_2Se_3 to moisture. In the full EBL fabrication, in addition to the exposure to moisture, we also find that the electron beam irradiation can dramatically increase the electron density.

To avoid those steps in device fabrication, we have

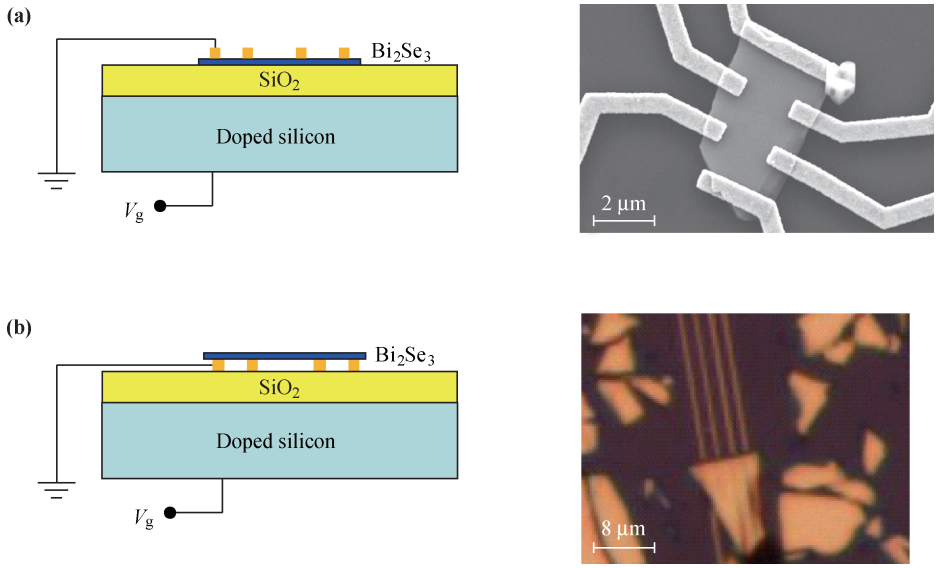

Fig. 4 **(a)** Schematic drawing of the EBL-fabricated device on SiO_2/Si substrate (*left*). Scanning electron microscope image of an EBL-fabricated optimally Ca-doped Bi_2Se_3 device (*right*). **(b)** Schematic drawing of the device prepared with the flake-on-top method described in the text (*left*). Optical microscope image of an optimally Ca-doped Bi_2Se_3 flake placed on top of a set of pre-patterned Au/Ti electrodes (*right*).

taken a different approach. We first prepare many sets of four parallel Au/Ti electrodes on a SiO_2/Si wafer. Then we exfoliate thin Bi_2Se_3 flakes and place them on the wafer. We search for good devices that contain only one flake bridging the four electrodes. An example is shown in Fig. 4(b). The contact resistance of the devices is typically $\sim$ 1 kΩ. Devices prepared in this method do not go through any baking, intentional exposure to polymer resist, moisture, or electron beam irradiation, and can be loaded to the measurement chamber immediately upon exfoliation and wire-bonding. The resistance vs. temperature curve shown in Fig. 5(a) in red clearly indicates an insulating behavior. Above $\sim$150 K, the resistance increases as the temperature is raised. This high temperature behavior may be expected for a degenerate electron (or hole) gas which results from a large number of thermally excited carriers at high temperatures. The temperature dependence of the resistivity is dominated by the electron–phonon scattering in this temperature range. Below 150 K, the rise in resistivity is caused by the freezing of the thermally excited carriers, which is finally taken over by a saturation behavior at lower temperatures. The residual conductivity at zero temperature can be attributed to the extended states such as the surface Dirac fermion states and/or the states in the impurity band, which are difficult to distinguish from each other from the resistivity data alone. In contrast to the EBL fabricated devices, this insulating device shows a reproducible peak in the gate voltage dependence [in Fig. 5(b)] of the saturation resistivity, which is reminiscent of the resistivity maximum in graphene at its Dirac point. However, the corresponding minimum conductivity value of this device is $\sim 50\ e^2/h$. If we attribute this minimum conductivity to the surface states, then each surface sheet would contribute to $\sim 25\ e^2/h$, which is still a factor of 10 larger than the graphene minimum conductivity. The origin of this large minimum conductivity is a subject of our ongoing investigations.

In summary, we have successfully realized the insulating state in both bulk Bi_2Se_3crystals and nanoscale

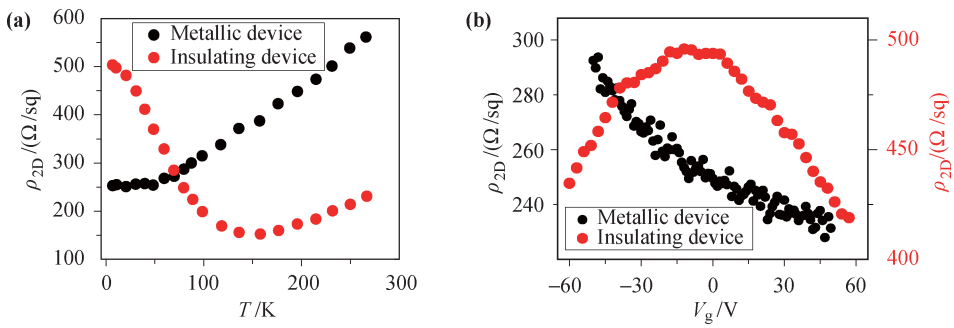

Fig. 5 **(a)** Electrical resistivity vs. temperature for an EBL-fabricated device (*black*) and a flake-on-top device (*red*). The former is clearly metallic and the latter insulating. **(b)** Gate voltage dependence of the two devices shown in (a) at 1.5 K. The red goes with the red scale and the black goes with the black scale.

devices which is critical to the transport studies of TIs. We have tuned the position of the Fermi level through the Dirac point in the band gap of Bi_2Se_3 by a combination of Ca-doping and electrostatic gating. In the gate-tunable devices, we have observed a minimum conductivity of $\sim 50\ e^2/h$, which is about an order greater than that in graphene at its Dirac point if it is solely caused by the surface Dirac states. The physical origin of the large minimum conductivity is currently being studied.

Acknowledgements We wish to thank V. Aji, X. F. Liu, T. Lin, and C. Varma for their assistance and useful discussions. This work was supported by the US Department of Energy, Office of Basic Energy Sciences, Division of Materials Sciences and Engineering under Award #DE-FG02-07ER46351.

References

1. H. J. Zhang, C. X. Liu, X. L. Qi, X. Dai, Z. Fang, and S. C. Zhang, Nat. Phys., 2009, 5(6): 438
2. Y. Xia, D. Qian, D. Hsieh, L. Wray, A. Pal, H. Lin, A. Bansil, D. Grauer, Y. S. Hor, R. J. Cava, and M. Z. Hasan, Nat. Phys., 2009, 5(6): 398
3. Y. L. Chen, J. H. Chu, J. G. Analytis, Z. K. Liu, K. Igarashi, H. H. Kuo, X. L. Qi, S. K. Mo, R. G. Moore, D. H. Lu, M. Hashimoto, T. Sasagawa, S. C. Zhang, I. R. Fisher, Z. Hussain, and Z. X. Shen, Science, 2010, 329(5992): 659
4. P. Roushan, J. Seo, C. V. Parker, Y. S. Hor, D. Hsieh, D. Qian, A. Richardella, M. Z. Hasan, R. J. Cava, and A. Yazdani, Nature, 2009, 460(7259): 1106
5. Y. S. Hor, A. Richardella, P. Roushan, Y. Xia, J. G. Checkelsky, A. Yazdani, M. Z. Hasan, N. P. Ong, and R. J. Cava, Phys. Rev. B, 2009, 79(19): 195208
6. J. G. Analytis, J. H. Chu, Y. L. Chen, F. Corredor, R. D. McDonald, Z. X. Shen, and I. R. Fisher, Phys. Rev. B, 2010, 81(20): 205407
7. D. X. Qu, Y. S. Hor, J. Xiong, R. J. Cava, and N. P. Ong, Science, 2010, 329: 821
8. Z. Wang, T. Lin, P. Wei, X. Liu, R. Dumas, K. Liu, and J. Shi, Appl. Phys. Lett., 2010, 97(4): 042112
9. J. G. Analytis, R. D. McDonald, S. C. Riggs, J. H. Chu, G. S. Boebinger, and I. R. Fisher, Nat. Phys., 2010, 6(12): 960
10. H. Köhler and A. Fabricius, Phys. Status Solidi (b), 1975, 71(2): 487
11. H. Köhler, Phys. Status Solidi (b), 1973, 58(1): 91